Signalome-wide mapping of the NFκB pathway in T-cells reveals novel targets for immunotherapy

Joseph Clarke[1], Haoqi Chen[2], Cristina Tormo Garcia[1], Ewa Basiarz[3], Mateusz Kotowski[1], Ana Mafalda Santos[1], Mai T Vuong[1], Paige Sherman[1], Jia Xin Li[1], Christopher J Tape[3#], Simon J Davis[1#], Evangelia Petsalaki[2#], Sumana Sharma[1#]

[1]Radcliffe Department of Medicine, John Radcliffe Hospital, University of Oxford, Oxford, OX3 9DS, United Kingdom

[2]European Molecular Biology Laboratory, European Bioinformatics Institute (EMBL-EBI), Wellcome Genome Campus, Hinxton, Cambridgeshire, CB10 1SD, United Kingdom

[3]Cell Communication Laboratory, Department of Oncology, University College London Cancer Institute, 72 Huntley Street, London, WC1E 6DD, United Kingdom

[#]Correspondence should be addressed to:

sumana.sharma@rdm.ox.ac.uk

petsalaki@ebi.ac.uk

simon.davis@imm.ox.ac.uk

c.tape@ucl.ac.uk

Abstract

Cell signalling networks govern fundamental cellular processes yet remain incompletely defined. Moreover, what is known is biased toward a limited subset of well-characterised components. Phosphoprotein-based interrogation methods, including mass spectrometry and targeted phosphosite panels, have limited utility in physiological settings dependent on cell–cell interactions because the signalling fluxes can be difficult to detect despite producing robust functional responses. Here we developed a perturbation-based experimental framework that infers signalling pathway architecture using quantitative functional outputs rather than direct measurements of effector state, e.g., phosphorylation levels. Using antigen-specific, NF-κB–GFP reporter-expressing transformed T-cells co-cultured with cellular targets, we performed an arrayed CRISPR–Cas9 screen targeting a curated signalome of kinases, phosphatases, adaptor and scaffolding proteins, totalling 700 genes. Quantitative effect-size profiling recovered canonical T-cell receptor regulators and revealed unequal, family-specific patterns of control over NF-κB activation. Comparing T-cell stimulation with low- and high-affinity antigen uncovered signal-strength-dependent buffering of proximal signalling nodes, exemplified by reduced sensitivity to perturbation of *LCK* under high-intensity stimulation. Targeted perturbation in primary human $CD8^+$ T-cells validated our findings and identified *TRRAP* and *CTDSPL2* as negative regulators of T-cell effector output, whose disruption enhanced cytotoxicity, degranulation, and cytokine production in both polyclonal and TCR-engineered T cells. Together, these results establish a scalable strategy for mapping signalling pathway architecture in the setting of physiological T-cell activation.

Introduction

Cellular signalling is crucial for fundamental processes such as growth, proliferation, differentiation, survival, metabolism, and specialised effector responses. Although powerful technologies such as CyTOF, LC–MS-based phosphoproteomics, and targeted phospho-panels have significantly advanced our ability to interrogate signalling events, our understanding of cellular signalling network structure and regulation remains incomplete. Moreover, current knowledge is disproportionately focused on a limited subset of well-studied components, leaving large portions of the signalling landscape poorly characterised.(*1*). This bias is particularly pronounced for kinases and phosphatases, the principal enzymatic drivers of signal transduction, for which an estimated 30-50% of cellular targets remain unknown, indicating that large regions of the signalling landscape remain unexplored (*2*).

Most contemporary approaches to studying signalling rely on direct measurement of molecular intermediates, most commonly phosphorylation events detected by antibody-based assays or mass spectrometry-based phosphoproteomics. Advances in enrichment-based LC-MS have enabled increasingly global profiling of signalling states (*3*–*8*), and these approaches have been extended through integration with genetic or pharmacological perturbations to infer causal relationships, exemplified by resources such as the Connectivity Map (CMap) (*9*). Despite these advances, molecular readout-based approaches remain limited in their ability to capture signalling behaviour under physiological conditions. They are biased toward abundant or highly dynamic phosphorylation events, require large numbers of cells, and rely heavily on curated pathway annotations for interpretation, reinforcing existing knowledge rather than revealing new regulatory logic. Consequently, signalling components that exert modest, distributed, or context-dependent effects on pathway output may be systematically overlooked.

These limitations are particularly pronounced in systems where signalling is spatially constrained and dependent on direct cell–cell interactions. Most phosphoproteomic and

kinase-activity-based studies are performed on bulk cell lysates, restricting their applicability in such contexts. T-cell activation exemplifies this challenge: apart from a small number of SILAC-based co-culture studies (*10–12*), much of the available signalling data relies on supraphysiological stimulation applied outside native cellular contexts to generate detectable responses (*5*, *13*). Single-cell approaches such as mass cytometry (CyTOF) partially address population averaging (*14–17*). However, these approaches also encounter biological limits. In direct T cell–target cell interactions, single-cell mass cytometric analyses reveal remarkably limited signalling flux, often indistinguishable from unstimulated states, in contrast to pharmacological induced T-cell activation (*18*). Notably, despite these modest detectable fluxes, T cells mount robust functional responses, indicating that phosphoprotein-based measurements fail to capture physiologically relevant signalling dynamics.

In contrast, functional outputs integrate signalling information over time and across molecular layers. This suggests an alternative strategy for interrogating signalling networks: rather than measuring signalling intermediates directly, signalling architecture can be inferred by systematically perturbing signalling components and quantifying their impact on downstream functional outputs.

Here, we implement this concept through a perturbation-based framework that reconstructs signalling dependencies directly from functional readouts. By combining arrayed CRISPR-Cas9-mediated gene disruption with a quantitative NF-κB reporter assay, we systematically interrogate the contribution of kinases, phosphatases, and adaptor proteins to signalling pathway transmission, and subsequent transcription factor activity, in a physiologically relevant, cell–cell interaction context. This approach enables quantitative assessment of graded effects across hundreds of signalling components, revealing how control is distributed across a signalling network rather than identifying only a small number of essential nodes.

Applying this strategy to T-cell receptor signalling, we generate a functional dependency map of NF-κB activation that reveals hierarchical control, distributed engagement across signalling

93 families, and context-dependent buffering of proximal signalling nodes as a function of ligand
94 affinity. Extending these findings to primary human $CD8^+$ T cells, we identify previously
95 unrecognized negative regulators of T-cell function, including TRRAP and CTDSPL2, whose
96 disruption enhances cytotoxic activity and effector responses. Together, this work establishes
97 a generalisable framework for reconstructing signalling architecture from functional outputs in
98 physiological contexts.

99 Results

100 A functional 1G4-TCR^+ Jurkat NF-kB reporter system enables analysis of T-cell
101 receptor signalling under physiological stimulation conditions.

102 To enable systematic interrogation of T-cell signalling through functional outputs, we
103 generated a Jurkat T-cell reporter line in which NF-κB activity is monitored via GFP expression
104 downstream of antigen-specific T-cell receptor (TCR) engagement. NF-κB was selected as a
105 core transcriptional output of T-cell activation, integrating signals from multiple proximal and
106 distal signalling pathways. Jurkat cells were first engineered to stably express an NF-κB-driven
107 GFP reporter (**Supplementary Fig. 1A-B)**. To ensure antigen-specific activation, endogenous
108 TCR expression was ablated by CRISPR targeting of *TRAC* and *TRBC*, and cells were
109 subsequently transduced with lentivirus encoding the 1G4 TCR (**Supplementary Figure 1C**),
110 which recognizes the cancer-testis antigen NY-ESO-$1_{157-165}$ (henceforth referred to simply as
111 NY-ESO-1) peptide presented by HLA-A*02:01, followed by introduction of constitutive Cas9
112 expression to facilitate CRISPR-Cas9-mediated genetic perturbation (**Supplementary Fig.
113 1D**).
114
115 This configuration establishes a defined receptor-ligand interaction that mimics physiological
116 T-cell-target cell engagement. When co-cultured with A375 melanoma cells pulsed with NY-
117 ESO-1 peptides, 1G4-TCR^+ Jurkat reporter cells exhibited robust NF-κB–dependent GFP

118 induction, whereas TCR-deficient parental cells remained unresponsive (**Fig. 1A–C**). Upon
119 the use of NY-ESO-1 altered peptide ligands (6T, 3Y, 3I and 9V) to initiate Jurkat T-cell
120 activation, GFP expression scaled with peptide affinity, demonstrating sensitivity across a
121 physiologically relevant range of TCR stimulation strengths (**Fig. 1B,C**).

122 To confirm that reporter activation reflected canonical TCR signalling, we genetically disrupted
123 key proximal signalling components. CRISPR-mediated targeting of established TCR
124 signalling mediators, including *LCP2* and *ZAP70*, significantly reduced NF-κB reporter activity
125 upon stimulation with both high- and low-affinity antigen (**Fig. 1D**). These results confirm that
126 NF-κB reporter activation depends on intact TCR-proximal signalling.

127 Together, these data establish a genetically tractable, antigen-specific Jurkat reporter system
128 that reliably converts physiologically relevant TCR engagement into a quantitative functional
129 readout of NF-κB activation. This platform provides a robust foundation for systematic
130 perturbation-based analysis of signalling dependencies in a cell–cell interaction context,
131 where direct phosphoprotein measurements are known to be challenging.

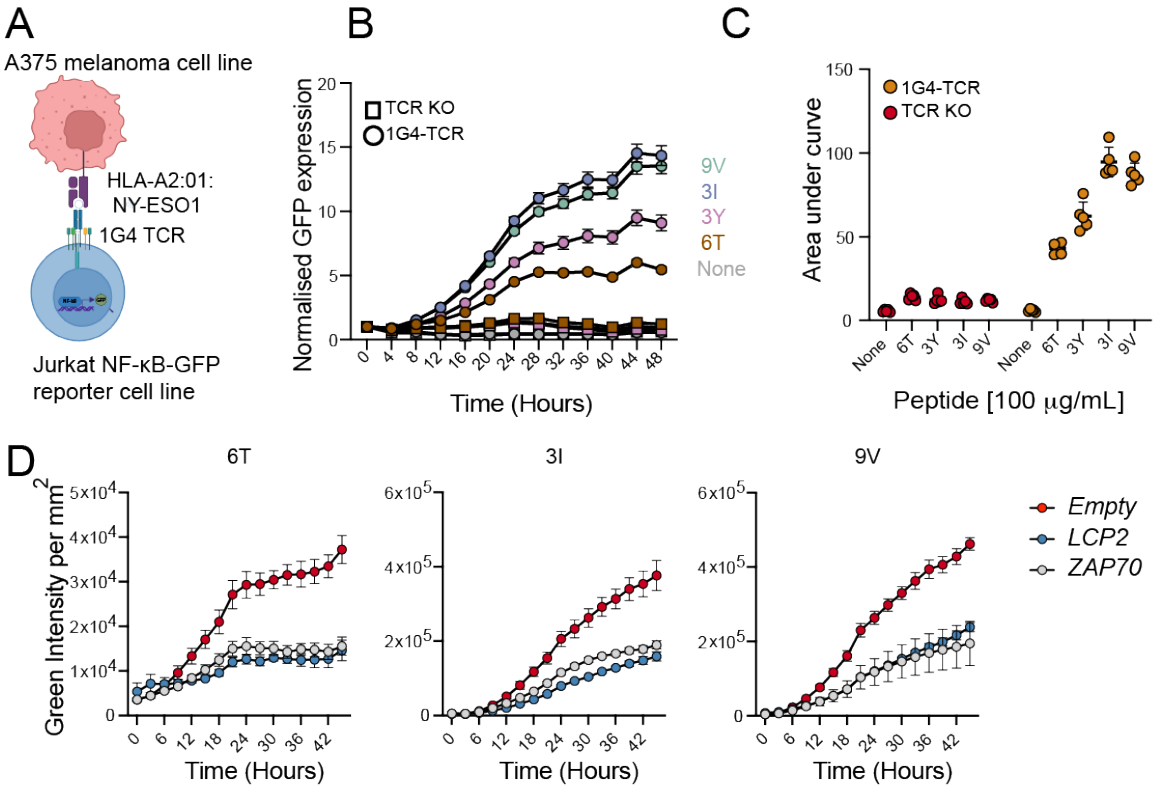

Figure 1: Establishing a peptide:MHC specific cell-cell interaction system to report functional activity of NFkB in T cells A: Schematic representing the co-culture system between Jurkat-NFkB-GFP reporter cell lines expressing the 1G4-TCR, and A375 melanoma cells pulsed with NY-ESO-1 peptides. **B:** Time course IncuCyte measurements of NFkB-GFP intensities from either 1G4-TCR^{+} Jurkat reporter lines (filled circles) or TCR-KO parental lines (filled squares). All NY-ESO-1 altered peptide ligands were used at final concentrations of 100µg/mL. **C:** Area under the curve (AUC) analysis of the data shown in panel B. **D:** Lentiviral sgRNA targeting of key TCR-signalling components *LCP2* or *ZAP70* in 1G4-TCR^{+} Jurkat reporters prevents GFP expression upon co-culture with NY-ESO-1 peptide pulsed A375 melanoma cells. All peptides were used at final concentrations of 100µg/mL, and time course GFP measurements were performed via IncuCyte imaging. All data shown from a minimum of three independent experiments.

A signalome-wide CRISPR-Cas9 screen reveals a quantitative map of NF-κB signalling in T cells

To enable systematic interrogation of T-cell signalling, we first defined a comprehensive "signalome" comprising kinases, phosphatases, and key adaptor proteins. We combined a curated list of 556 human kinases with 136 protein phosphatases defined by the HUGO Gene

152 Nomenclature Committee (*19*), and filtered this set for genes expressed across multiple
153 immune and cancer cell models using bulk RNA-seq data from Cell Model Passports (TPM >
154 0.3; Jurkat, MOLT-4, Daudi, THP-1, and two colorectal cancer organoids) (*20*). To further
155 enrich for signalling components relevant to T cells, we included genes annotated in KEGG
156 pathways associated with TCR signalling, JAK-STAT, calcium signalling, actin regulation,
157 phosphatidylinositol signalling, and MAPK signalling (*21*), as well as all genes encoding for
158 SH2 domain-containing proteins, to ensure coverage of adaptor and scaffolding molecules.
159 This yielded a final library of 708 genes, each targeted with two sgRNAs for CRISPR-Cas9-
160 mediated perturbation (**Supplementary Table 1**).
161
162 To place this signalome in the context of existing knowledge, we integrated transcriptional and
163 perturbation-based datasets from diverse T-cell contexts. Analysis of published expression
164 datasets spanning multiple activation timepoints in $CD8^+$ and pan-T cells (*22–25*) revealed
165 that 440 signalome genes are dynamically regulated at the transcriptional level (**Fig. 2A;**
166 **Supplementary Table 2**). In parallel, we mapped hits from published genome-wide CRISPR
167 loss-of-function and gain-of-function screens in T cells (*26–29*) onto the signalome (**Fig. 2B;**
168 **Supplementary Table 2**). Across these datasets, 63 genes were identified in loss-of-function
169 screens and 49 in gain-of-function screens. Genes implicated by CRISPR perturbation were
170 significantly enriched for genes encoding SH2-domain-containing proteins ($p = 2x10^{-5}$, Fisher's
171 exact test), underscoring their central role in T-cell signalling. Notably, 36 genes that were not
172 transcriptionally regulated nonetheless exhibited functional effects in CRISPR screens,
173 including seven core T-cell signalling genes encoding for SH2-domain-containing proteins
174 (CBLB, GRB2, ZAP70, SLA2, CBL, LCP2, VAV1), whereas many transcriptionally regulated
175 signalling genes were not detected in pooled CRISPR screens, highlighting potential gaps in
176 existing perturbation-based maps (**Fig. 2A,B**).
177
178 We next performed a signalome-wide, arrayed CRISPR perturbation screen to directly quantify
179 the contribution of each component to NF-κB activation. 1G4-TCR^+ Jurkat reporter cells were

transduced with individual sgRNAs and stimulated through cell–cell co-culture with peptide-pulsed target cells. In total, ~1,500 sgRNAs targeting ~700 genes were assayed in 96-well format across 13 experimental batches (**Fig. 2C**). Each batch included internal controls, including an empty sgRNA vector and sgRNAs targeting known TCR signalling components (*LCP2, ITK*), enabling normalization of gene-level effects based on GFP signal area under the curve (AUC) relative to empty controls and an internal positive control to assess the editing efficiency (**Methods**).

The screen showed high technical robustness. Independent sgRNAs targeting the same gene exhibited strong concordance, with ~80% of guide pairs showing consistent effect direction (**Fig. 2D; Supplementary Figure. 2A**). Gene-level effects were highly correlated for T-cell stimulation with low-affinity (6T) and high-affinity (9V) antigens (Spearman $\rho = 0.92$), indicating that the core signalling architecture governing NF-κB activation is largely conserved across stimulation strengths (**Fig. 2E**). Most genes clustered near the identity line, whereas a subset showed context-dependent deviations. Notably, disruption of *LCK* and *PRKCQ* strongly attenuated NF-κB activation under weak stimulation but had a markedly reduced effect under high-affinity stimulation (**Supplementary Figure. 2B**), consistent with partial bypass or compensation at higher signalling strength (*30*, *31*).

To characterize the global structure of signalling control, we ranked genes by their mean effect size across both conditions. The distribution was strongly skewed toward negative effects, consistent with depletion-driven signalling dependencies rather than enrichment effects (**Fig. 2F**). Canonical TCR signalling components, including *LCK, ZAP70, ITK, and LCP2*, ranked among the strongest negative regulators, validating the ability of this approach to recover core pathway architecture (**Fig. 2F**). TCR-specific signalling was among the highest-ranked pathways in the enrichment analysis, suggesting that the screen successfully recapitulated known genes while also assigning quantitative scores to signalome genes involved in regulating the NF-κB pathway (**Supplementary Figure 2C**).

207 We next examined how signalling control was distributed across protein families by comparing
208 effect size distributions within each family (**Fig. 2G**). All families contributed to NF-κB
209 regulation, but with distinct patterns. SH2-domain-containing proteins exhibited broad effect
210 size distributions, indicating distributed engagement of multiple family members. In contrast,
211 MAP kinase contributions were concentrated in a small number of nodes, leading towards
212 ERK1/2 (*MAPK3/MAPK1*) and p38α (*MAPK14*) (**Fig 2F, H**). These patterns suggest that NF-
213 κB signalling integrates both distributed adaptor-mediated control and more focal kinase
214 bottlenecks, rather than being uniformly dominated by single components. Based on these
215 quantitative dependencies, we reconstructed a data-driven network representation of NF-κB
216 regulation, capturing hierarchical patterns of control, characterized by a small number of high-
217 impact nodes alongside broadly distributed contributions from adaptor families (**Fig. 2H;**
218 **Supplementary Table 2**).

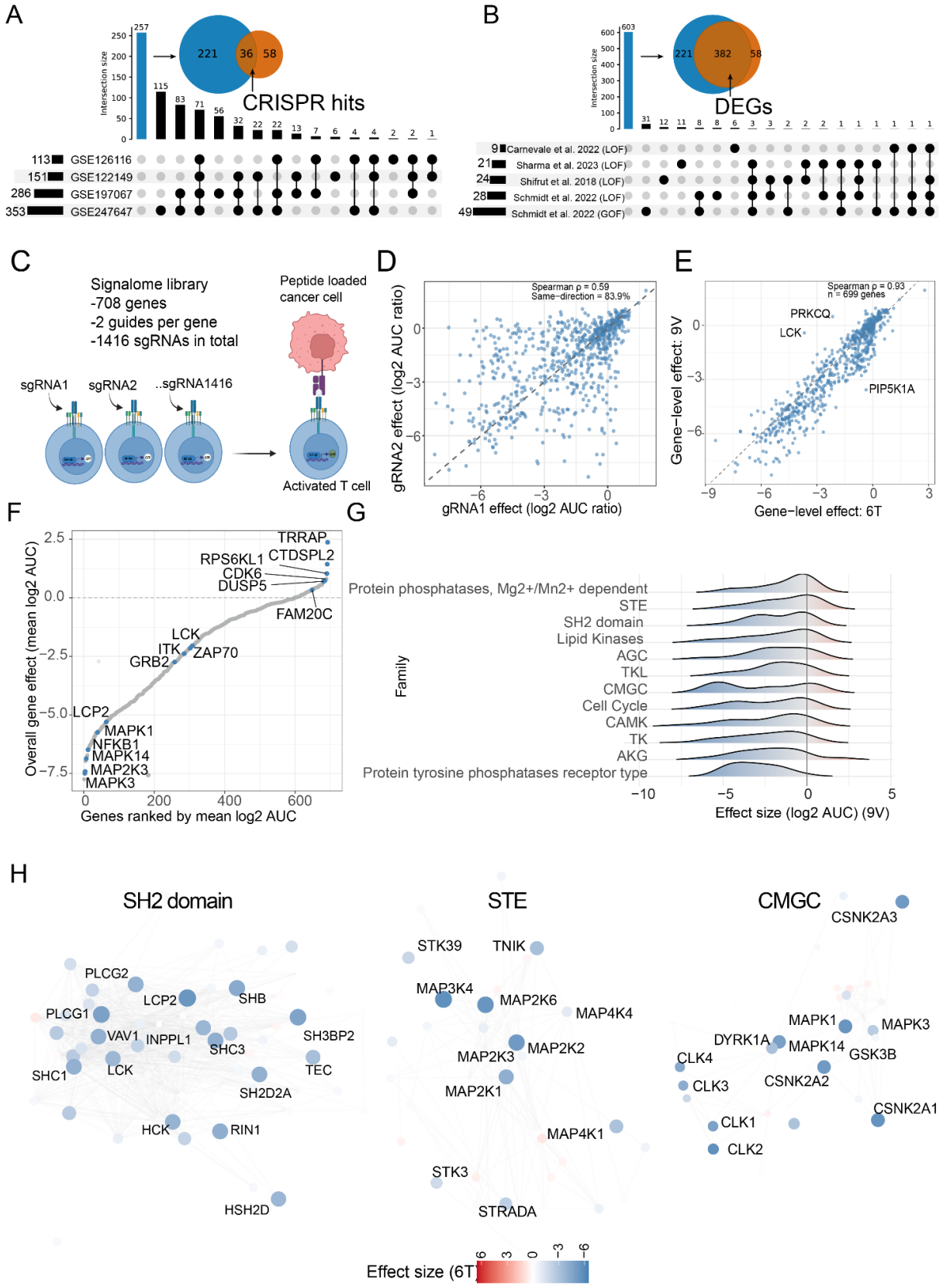
A
Intersection size
257
115
83
71
56
32
22
22
13
7
6
4
4
2
2
1
221
36
58
CRISPR hits
113 GSE126116
151 GSE122149
286 GSE197067
353 GSE247647
B
Intersection size
603
31
12
11
8
8
6
3
3
2
2
2
1
1
1
1
1
1
221
382
58
DEGs
9 Carnevale et al. 2022 (LOF)
21 Sharma et al. 2023 (LOF)
24 Shifrut et al. 2018 (LOF)
28 Schmidt et al. 2022 (LOF)
49 Schmidt et al. 2022 (GOF)
C
Signalome library
-708 genes
-2 guides per gene
-1416 sgRNAs in total
sgRNA1
sgRNA2
..sgRNA1416
Peptide loaded cancer cell
Activated T cell
D
Spearman ρ = 0.59
Same−direction = 83.9%
gRNA2 effect (log2 AUC ratio)
gRNA1 effect (log2 AUC ratio)
E
Spearman ρ = 0.93
n = 699 genes
PRKCQ
LCK
PIP5K1A
Gene−level effect: 9V
Gene−level effect: 6T
F
Overall gene effect (mean log2 AUC)
TRRAP
RPS6KL1
CTDSPL2
CDK6
DUSP5
FAM20C
LCK
ITK
ZAP70
GRB2
LCP2
MAPK1
NFKB1
MAPK14
MAP2K3
MAPK3
Genes ranked by mean log2 AUC
G
Protein phosphatases, Mg2+/Mn2+ dependent
STE
SH2 domain
Lipid Kinases
AGC
TKL
CMGC
Cell Cycle
CAMK
TK
AKG
Protein tyrosine phosphatases receptor type
Family
Effect size (log2 AUC) (9V)
H
SH2 domain
PLCG2
LCP2
SHB
PLCG1
VAV1
INPPL1
SHC3
SH3BP2
SHC1
LCK
TEC
SH2D2A
HCK
RIN1
HSH2D
STE
STK39
TNIK
MAP3K4
MAP2K6
MAP4K4
MAP2K3
MAP2K2
MAP2K1
MAP4K1
STK3
STRADA
CMGC
CSNK2A3
MAPK1
MAPK3
DYRK1A
MAPK14
GSK3B
CLK4
CSNK2A2
CLK3
CSNK2A1
CLK1
CLK2
Effect size (6T)

219

220

221 **Figure 2: A signalome-wide, arrayed CRISPR perturbation screen reveals hierarchical**
222 **and distributed control of NF-κB signalling in T cells**. **A:** Overlap between genes that are
223 not transcriptionally regulated across four T-cell–specific expression datasets and genes
224 identified as hits in genome-wide CRISPR screens, revealing 36 signalling genes that are
225 functionally required despite lacking dynamic expression changes. UpSet plot shows
226 intersections across expression studies. **B:** Overlap between genes that are differentially
227 expressed in at least one T-cell expression dataset and genes not identified as hits in genome-
228 wide CRISPR screens, identifying 382 signalling genes that are transcriptionally regulated but
229 not functionally required in pooled CRISPR screens. UpSet plot shows intersections across
230 CRISPR studies. **C:** Schematic of the arrayed CRISPR perturbation strategy. **D:** Concordance
231 between independent sgRNAs targeting the same gene under high-affinity stimulation (9V).
232 Each point represents a gene; axes show $\log_2$(AUC ratio) for sgRNA1 versus sgRNA2. **D:**
233 Comparison of gene-level perturbation effects between low-affinity (6T) and high-affinity (9V)
234 stimulation conditions. Each point represents one gene collapsed across sgRNAs. **F.** Genes
235 ranked by overall effect size, defined as the mean gene-level $\log_2$(AUC ratio) across both
236 stimulation conditions. **G:** Distribution of absolute effect sizes stratified by functional protein
237 families **H:** Network representation of selected signalling modules with node colour indicating
238 signed effect size under stimulation with high-affinity antigen (9V). Nodes represent genes;
239 edges correspond to curated functional interactions.

240 Targeted perturbation of SH2-domain-containing proteins in primary CD8$^+$ T cells
241 validates functional TCR signalling dependencies

242 Although large-scale perturbation screens with functional read outs are readily implemented
243 in cell lines, extending such approaches to primary human T cells remains challenging. To
244 enable arrayed perturbation in primary CD8$^+$ T cells at scale, we established a workflow based
245 on lentiviral delivery of sgRNAs followed by Cas9 electroporation, a strategy compatible with
246 systematic perturbation, while avoiding the cost and scalability constraints of RNP-only
247 approaches (*27*).

248 A further barrier to scalable functional assays in primary T cells is antigen specificity, as
249 individual T cells respond only to their cognate TCR ligand. To circumvent this limitation, we
250 employed bispecific molecules, which engage CD3 independently of endogenous TCR
251 specificity (*32*, *33*). Here, the bispecific engager consists of an anti-CD3 single-chain variable
252 fragment fused to a TCR targeting an HLA-A2-bound gp100 peptide (YLEPGPVTV), thereby
253 triggering TCR signalling and directing T-cell activation against gp100-pulsed A375 melanoma
254 cells (*18*). This approach enables the use of polyclonal primary CD8$^+$ T cells while preserving

255 physiologically relevant TCR-proximal signalling, thus substantially increasing experimental
256 scalability.

257 Upon co-culture with gp100-pulsed target cells, polyclonal $CD8^+$ T cells exhibited robust
258 upregulation of activation markers (CD69, CD25, 4-1BB) and potent cytotoxicity (**Fig. 3A**).
259 Despite these strong functional responses, phosphoprotein changes measured by CyTOF
260 remained limited (**Fig. 3B, Supplementary Figure 3**), consistent with the low signalling flux
261 observed during direct cell–cell interactions and reinforcing the sensitivity of functional
262 readouts for capturing signalling outcomes (*18*).

263 To validate the signalling architecture inferred from the Jurkat signalome screen in a
264 physiological setting, we focused on the SH2-domain-containing protein family, which
265 exhibited broad functional engagement in NF-κB regulation despite lacking a coherent pattern
266 of transcriptional regulation during T-cell activation (**Fig. 2G**). This family includes multiple
267 well-established TCR signalling components, making it a suitable test case for functional
268 validation. We targeted 66 SH2-domain-containing genes, along with control targets, in
269 polyclonal primary $CD8^+$ T cells from six independent donors using lentiviral sgRNA delivery
270 followed by Cas9 electroporation (**Supplementary Figure 4A**). Functional consequences
271 were assessed by quantifying target cell killing in co-culture assays (**Fig. 3C**).

272 Disruption of canonical TCR signalling components, including *LCK*, *LCP2*, and *ITK*, markedly
273 impaired $CD8^+$ T-cell cytotoxicity (**Fig. 3C,D**) and reduced expression of activation markers 4-
274 1BB (**Fig. 3E**) and CD25 (**Supplementary Figure 4B**) at 48 hours, validating the sensitivity
275 and specificity of the assay. After correcting for donor and batch effects (**Methods**), systematic
276 perturbation of the SH2 gene family revealed a spectrum of functional effects on cytotoxicity
277 **(Fig. 3F)**.

278 Genes were ranked by their impact on tumour cell killing, with cytotoxicity levels quantified
279 using the AUC metric (**Methods**). Our analysis revealed profiles that closely mirrored both
280 known TCR signalling annotations, and the dependencies observed in the Jurkat screen (**Fig.**

281 **3F**). Perturbation of key signalling mediators (*ITK*, *LCK*, *LCP2*, *PLCγ*, *PIK3R1-3*), adaptor
282 proteins (*GRAP*, *GRB2*), and cytoskeletal regulators (*VAV1*, *VAV3*) consistently reduced
283 $CD8^+$ T-cell cytotoxicity, whereas disruption of *SLA2* and *PTEN*, both known negative
284 regulator of TCR signalling, enhanced $CD8^+$ T-cell-mediated killing (**Fig. 3G; Supplementary**
285 **Fig. 4C,D**). These results demonstrate that the SH2 gene family constitutes a distributed and
286 functionally essential regulatory module in primary T-cell activation.

287 Because bispecific-based activation bypasses endogenous antigen specificity, we next asked
288 whether these dependencies were preserved in antigen-specific TCR-engineered T cells.
289 Primary $CD8^+$ T cells were transduced with plasmids encoding the 1G4-TCR and an LNGFR
290 tag, and TCR Vβ13.1$^+$ $LNGFR^+$ cells were sorted and expanded for use *in vitro*
291 (**Supplementary Fig. 4E**). This system enabled direct comparison of signalling requirements
292 across different ligand affinities. Consistent with the Jurkat screen, disruption of *LCK* exhibited
293 affinity-dependent effects: under high-affinity stimulation with the 3Y peptide, *LCK* targeting
294 had minimal impact on tumour cell killing, whereas under weaker stimulation conditions (6T),
295 cytotoxicity was strongly impaired (**Fig. 3G**).

296 Together, these results demonstrate that functional signalling dependencies identified in
297 Jurkat cells are largely conserved in primary human $CD8^+$ T cells. This validation establishes
298 the robustness of the perturbation-based framework across experimental systems and
299 highlights how distributed adaptor-mediated regulation and signal-strength–dependent
300 buffering shape TCR-driven functional responses.

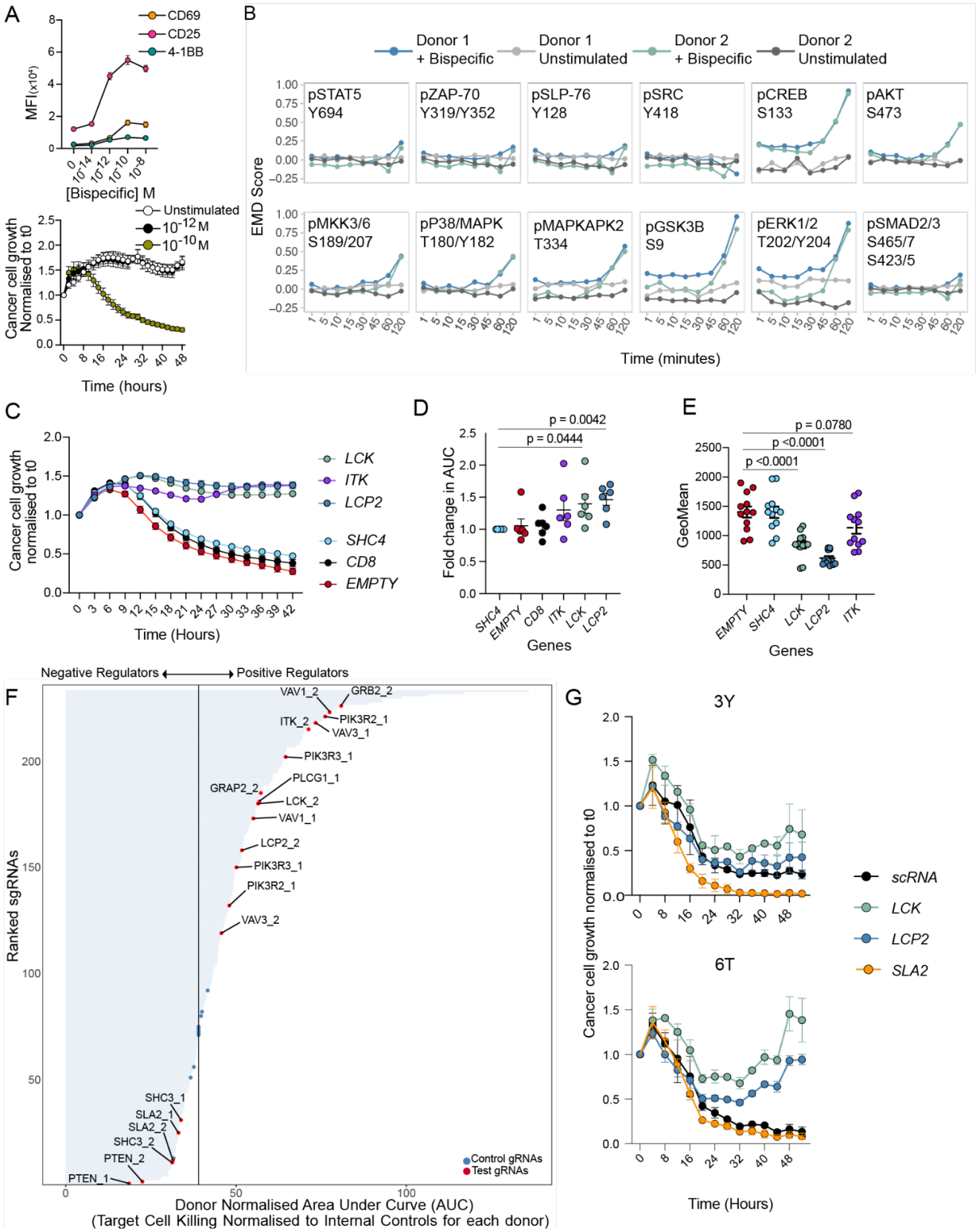

Figure 3: Targeted perturbation in primary CD8⁺ T-cells reveals the spectrum of activity of the SH2 gene family on T-cell cytotoxicity. A: Top panel - Expression (mean fluorescence intensity, MFI) of activation markers on CD8⁻ T-cells at 24 hours following co-

305 culture with gp100 pulsed A375 melanoma cell lines and a bispecific T cell engager. Bottom
306 panel - $CD8^+$ cytotoxic responses following co-culture with A375 melanoma cell lines as
307 described for the top panel. Data in both panels from 3 independent donors, representative of
308 at least 3 experimental repeats. **B:** Phosphorylation of early signalling mediators downstream
309 of TCR engagement as measured by mass cytometry (CyTOF). Data shown from two
310 independent donors in one experiment, representative of at least 4 independent donors across
311 4 experiments. **C:** Representative killing curves from $CD8^+$ T-cell co-cultures with A375
312 melanoma cells. T-cell activation was initiated through use of the bispecific engager at a final
313 concentration of 10^{-10}M. Targeting of known TCR-signalling mediators with sgRNAs inhibits
314 cytotoxic T-cell responses. Data show from one donor and one independent experiment,
315 representative of at least 6 independent donors across 6 independent experiments. **D:** Area
316 under the curve (AUC) analysis of killing curves shown in panel C, normalised to SHC4
317 targeted controls. Data from 6 independent donors across 6 independent experiments.
318 Statistical analysis performed by paired T-test. **E:** Targeting TCR-signalling mediators with
319 sgRNAs reduces surface 4-1BB expression, measured at 48 hours post co-culture with A375
320 melanoma cells as detailed in D. Data shown are the same T-cells from panel D, and are from
321 6 independent $CD8^+$ donors across 6 independent experiments. Statistical analysis performed
322 via One-Way ANOVA with Dunnett's multiple comparison tests. **F:** Waterfall plot of normalised
323 AUCs from killing curves illustrated in panel C, from experiments targeting all genes encoding
324 SH2-domain containing proteins. Killing curves for each perturbation were first normalised to
325 donor-specific internal negative control sgRNAs before computing AUC values. Ranked gene
326 analysis identifies both positive and negative regulators of T-cell cytotoxicity within the SH2
327 gene family. **G:** Representative killing curves from targeting *LCK*, *LCP2* or *SLA2* in primary
328 1G4-TCR^+ $CD8^+$ T-cells. A375 melanoma cell lines were pulsed with NY-ESO-1 peptides as
329 indicated to final concentrations of 100µg/mL. Data shown from one independent experiment,
330 representative of two independent repeats using two individual $CD8^+$ donors.

331 *TRRAP* and *CTDSPL2* constrain $CD8^+$ T-cell effector output downstream of TCR 332 signalling

333 Although the majority of perturbations in the signalome screen reduced NF-κB activity, a small
334 number of gene disruptions increased reporter output. Among these, targeting of *TRRAP* and
335 *CTDSPL2* consistently enhanced NF-κB-driven GFP expression in Jurkat cells (**Fig. 4A**).
336 TRRAP is a pseudokinase that functions as a scaffold within histone acetyltransferase
337 complexes involved in transcriptional regulation, whereas CTDSPL2 is a poorly characterized
338 serine/threonine phosphatase. Neither protein has been well defined in the context of T-cell
339 signalling, prompting further functional validation in primary cells.

340

341 To assess their roles in physiological settings, we targeted *TRRAP* or *CTDSPL2* in primary
342 human $CD8^+$ T cells using lentiviral sgRNA delivery followed by Cas9 electroporation.

343 Disruption of either gene significantly enhanced CD8$^+$ T-cell-mediated killing of A375
344 melanoma cells in bispecific-based co-culture assays (**Fig. 4B**). Consistent with increased
345 effector activity, targeting *TRRAP* or *CTDSPL2* also elevated IFNγ secretion at 24 hours (**Fig.**
346 **4C**). In addition, after targeting *TRRAP* or *CTDSPL2* we observed enhanced degranulation,
347 as measured by surface CD107α expression at 4 hours post A375 co-culture (**Fig. 4D**). These
348 results indicate that both proteins act to constrain T-cell effector responses downstream of
349 TCR-proximal signalling.
350
351 Because bispecific-based activation bypasses endogenous antigen specificity, we next
352 examined whether these effects were preserved in antigen-specific TCR-engineered T cells.
353 Primary CD8$^+$ T cells expressing the 1G4 TCR were electroporated with sgRNA–Cas9
354 ribonucleoprotein (RNP) complexes targeting *TRRAP* or *CTDSPL2*, and cytotoxic activity was
355 assessed against A375 melanoma cells presenting endogenous levels of NY-ESO-1.
356 Importantly, these experiments utilised a distinct, non-overlapping sgRNA sequence
357 compared to these utilised in our signalome-wide arrayed screen. Under these basal antigen
358 conditions, disruption of either gene significantly enhanced tumour cell killing relative to
359 scrambled controls (**Fig. 4E**). This enhancement was maintained across a range of peptide
360 affinities, again utilising 6T or 3Y NY-ESO-1 altered peptide ligands (**Supplementary Fig. 5A**).
361
362 Finally, to assess whether enhanced CD8$^+$ T-cell effector functions arising from *TRRAP* or
363 *CTDSPL2* perturbations were accompanied by an increase in markers of T-cell dysfunction
364 and exhaustion (e.g., PD-1, LAG-3 and TIM-3), cell surface expression of these molecules
365 was assessed in polyclonal CD8$^+$ T-cells 24 hours post stimulation with A375 melanoma cells
366 and the bispecific engager. Phenotypically, *TRRAP* or *CTSPL2* targeted T-cells were similar
367 to the unedited, empty plasmid controls, where expression of these three inhibitory receptors
368 displayed an activation-marker-like expression pattern. Expression of surface PD-1, LAG-3
369 and TIM-3 all correlated with the bispecific concentration utilised to initiate T-cell activation in

370 these experiments, and reduced expression was observed in the *LCP2* targeted control
371 (**Supplementary Fig. 5B**).

372 To investigate how TRRAP and CTDSPL2 depletion enhanced cytotoxicity, we performed
373 RNA sequencing following CRISPR-mediated perturbation in primary $CD8^+$ T-cells. TRRAP is
374 a scaffold component of the SAGA and TIP60 histone acetyltransferase complexes and
375 supports MYC- and E2F-dependent transcriptional programs. Consistent with this role, upon
376 activation, TRRAP-deficient T cells exhibited coordinated downregulation of genes associated
377 with cell cycle progression and DNA replication, including CENPA, PLK1, POLE2, and multiple
378 MCM complex components. In contrast, inflammatory and immune signalling genes, including
379 IFITM5, IL23R and NR4A family components were upregulated (**Figure 4F, Supplementary**
380 **Table 3**). Pathway-level analysis revealed suppression of proliferative programs alongside
381 enrichment of inflammatory and cytokine signalling modules (**Figure 4G**). These findings
382 suggest that TRRAP loss shifts T cells away from a proliferative transcriptional state toward
383 an inflammatory, effector-associated profile. By contrast, CTDSPL2-deficient cells displayed
384 minimal global transcriptional remodelling. Donor-paired analyses demonstrated that most
385 genes remained near baseline at both stimulated and unstimulated conditions
386 (**Supplementary Fig. 5C, Supplementary Table 3**). The increased killing arising from
387 *CTDSPL2* perturbation is, therefore, unlikely to arise from large-scale transcriptional
388 reprogramming and instead reflects altered signalling dynamics.

389 Together, these data identify TRRAP and CTDSPL2 as previously unrecognized negative
390 regulators of $CD8^+$ T cell effector function. Their disruption enhances cytotoxicity, cytokine
391 production, and degranulation under both polyclonal and antigen-specific activation conditions
392 without inducing excessive expression of inhibitory receptors. These findings highlight novel
393 regulatory nodes that may be therapeutically leveraged to enhance T cell–based
394 immunotherapies.

395

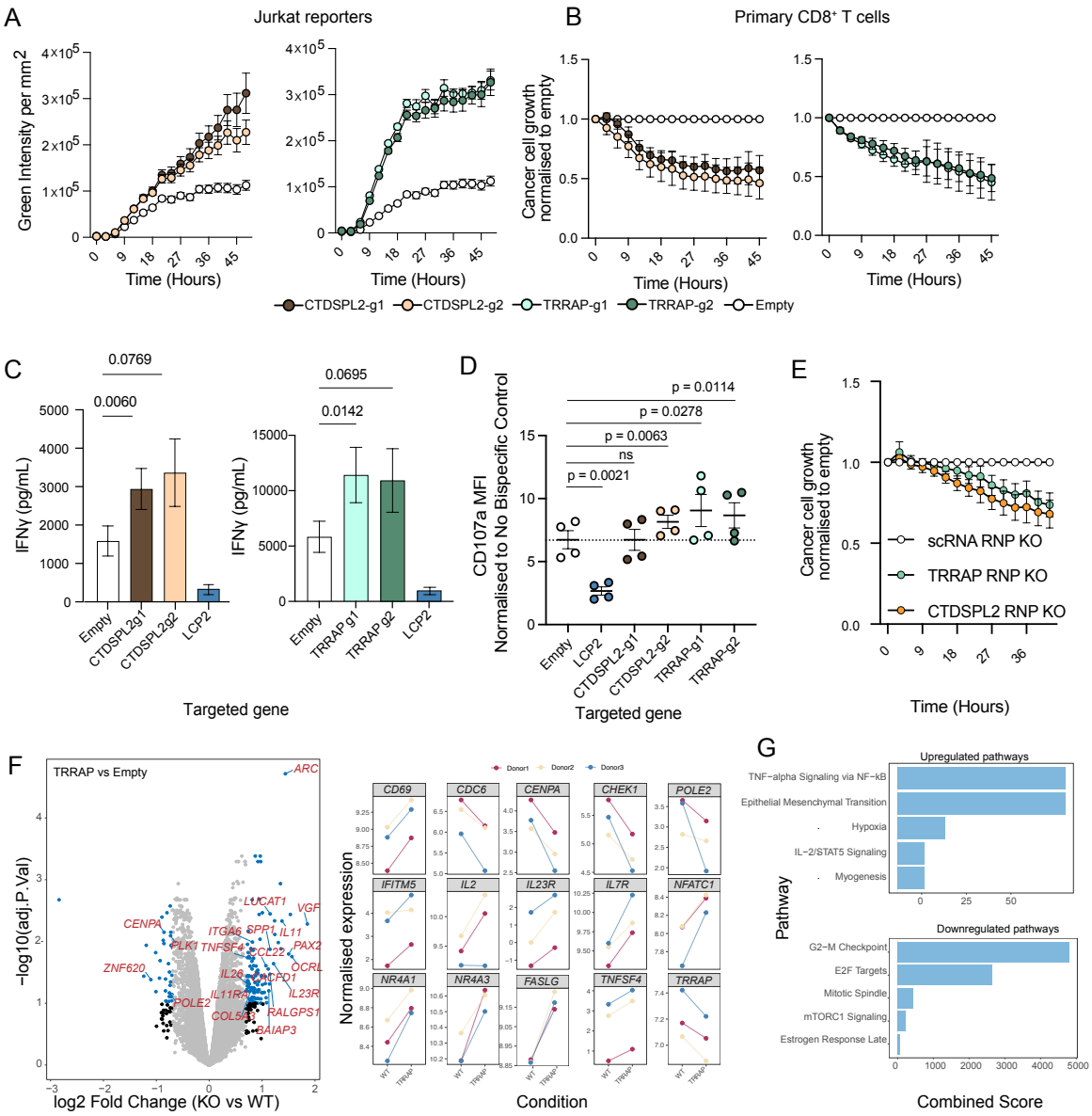

Figure 4: Perturbation of novel targets *CTDSPL2* and *TRRAP* enhances primary CD8⁺ T-cell functional activity. A: NFkB-GFP traces from 1G4-TCR⁺ Jurkat reporters when transduced with *CTDSPL2* (left) or *TRRAP* targeting sgRNAs (right). Jurkat cells were stimulated with A375 melanoma cell lines pulsed with NY-ESO-1 9V peptide (100µg/mL). **B:** Cytotoxic responses from primary CD8⁺ T-cells when co-cultured with A375 melanoma cell lines pulsed with gp100 peptide and a bispecific T-cell engager (final concentration 10^{-11}M). Data shown from 9 independent donors across 3 experiments (TRRAP sgRNAs) or a minimum of 4 independent donors across 2 experiments (CTDSPL2 sgRNAs). A375 cell growth was normalised to the empty control for each donor. **C:** IFN_{γ} secretion at 24 hours from primary CD8⁺ T-cells stimulated as described for panel B. Data shown from 2 independent donors across 1 individual experiment, representative of at least 4 independent donors across 2 experiments. Statistical analysis performed via One-Way ANOVA with Dunnett's multiple comparisons. **D:** CD107α mean fluorescence intensity (MFI) from CD8⁺ T-cells stimulated as described for panel B, measured at 4 hours post stimulation. CD107a expression was normalised to unstimulated controls (no bispecific) for each CRISPR targeting condition. Data

shown from 4 independent donors across 2 experiments. **E:** Cytotoxic responses of 1G4-TCR$^+$ primary CD8$^+$ T-cells when co-cultured with A375 melanoma cell lines expressing basal NY-ESO-1. 1G4-TCR$^+$ CD8$^+$ T-cells were electroporated with RNPs targeting either *CTDSPL2* or *TRRAP*, together with a scrambled control (scRNA). Data shown from 6 donors across 3 independent experiments. Growth curves were normalised to the scRNA controls for all donors. **F.** Differential gene expression analysis of *TRRAP*-targeted primary CD8$^+$ T cells following stimulation. Volcano plot showing $\log_2$ fold change (KO vs WT) versus $-\log_{10}$ adjusted P value from donor-controlled limma-voom analysis (n = 3 donors). Selected representative genes are highlighted. Inset panels show donor-resolved normalized expression for representative upregulated inflammatory genes (e.g., IL2, IL7R, IL23R, TNFSF4) and downregulated proliferative genes (e.g., CDC6, CENPA, CHEK1, POLE2). Lines connect paired donor samples. TRRAP transcript abundance was modestly but consistently reduced across donors (see Fig. 4F, inset). **G**. Pathway enrichment analysis of differentially expressed genes in *TRRAP*-targeted cells. Hallmark gene set enrichment (Enrichr) identified suppression of proliferative programs, including G2/M checkpoint and E2F target pathways, and enrichment of inflammatory and TNFα–NF-κB signalling modules. Combined enrichment scores are shown.

Discussion

In this study, we present a perturbation-based framework to interrogate cellular signalling during physiological cell–cell engagement. Leveraging functional readouts rather than direct measurement of signalling intermediates allowed us to identify key signalling regulators despite remarkably low signalling flux under these conditions (*18*). By quantifying transcription factor activity following systematic perturbation of signalling components, we could capture pathway activity through integrated transcriptional outputs rather than discrete molecular states. This approach is motivated by models of temporal signal integration, as articulated by Purvis and Lahav, and by subsequent optogenetic studies demonstrating that many proximal T-cell signalling intermediates decay rapidly following receptor disengagement (*34*, *35*). In contrast, transcriptional outputs integrate signalling over time, accumulating to provide a longer-lived functional record of signalling activity. In the context of T-cell activation, our findings support this framework by demonstrating that robust NF-κB activation and effector responses results from low-amplitude or spatially restricted signalling during direct T-cell-tumour cell engagement.

444 A key feature of this framework is its compatibility with physiologically relevant stimulation
445 formats. By interrogating signalling in cell–cell co-culture systems, our approach avoids
446 reliance on supraphysiological stimulation commonly required to elicit detectable changes in
447 phosphorylation or kinase activity, and instead captures the integration of complex signal
448 inputs that arise during direct cellular interactions. Although strong stimulation (most often
449 achieved using anti-CD3/CD28 bead-based activation) has been instrumental for defining
450 canonical signalling pathways in global phosphoproteomic studies (*3*, *5*, *11*), it may not reflect
451 signalling behaviour in physiological settings. This limitation is particularly relevant in studies
452 of T-cell activation, where signalling outcomes reflect the combined influence of antigen
453 affinity, co-stimulatory, and inhibitory inputs, such that maximal pathway activation cannot be
454 assumed to be an appropriate starting point for interrogating authentic signalling processes.
455 Similar considerations apply to high-dimensional single-cell approaches, including mass
456 cytometry, which have provided powerful insights when phosphorylation flux is sufficiently
457 robust, but which typically rely on maximal signalling to infer signalling relationships (*17*, *36*).

458 Applying this strategy to T-cell receptor signalling revealed that the nodes important for
459 functional signalling are largely unchanged at different stimulation strengths produced by
460 differing-quality TCR ligands, whereas there do exist specific nodes that are highly context
461 dependent. In particular, perturbation of *PKRCQ* and *LCK* exhibited a strong dependence on
462 ligand affinity; disruption of both markedly impaired NF-κB activation under weak stimulation
463 but was buffered under high-intensity conditions. PKCθ is proposed to function as a signal
464 amplifier downstream of the TCR, particularly under conditions of limiting stimulation (*31*).

465 Similarly, quantitative modulation of proximal kinase activity has been described for LCK.
466 Partial reduction of LCK activity preferentially impairs T cell responses to low-affinity or low-
467 dose antigen, whereas strong stimulation can partially compensate for diminished kinase
468 availability (*30*, *37*, *38*). Notably, Cabezas-Caballero and colleagues demonstrated that
469 altering coreceptor identity (swapping CD8 and CD4) effectively redistributes and sequesters
470 LCK, thereby tuning TCR sensitivity by modulating the local availability of active kinase. This

work highlights how LCK availability functions as a quantitative regulator of signalling output. Together, these findings outline how targeting key proximal signalling components can serve as a mechanism to engineer tuning of cellular signalling in the context of varied stimulation strengths.

Beyond individual nodes, our data reveal how signalling control is unequally distributed across molecular families. Rather than treating pathway components as interchangeable, our perturbation-based analysis quantifies family-level engagement, distinguishing signalling nodes dominated by a small number of high-impact components from those that rely on distributed contributions. This is exemplified by the MAPK pathway, in which NF-κB regulation was driven primarily by a limited set of kinases, consistent with bottlenecked enzymatic cascades. In contrast, SH2-domain–containing proteins exhibited broad functional engagement, reflecting their role as proximal adaptors that integrate receptor-derived signals and connect them to diverse downstream pathways. These patterns are consistent with the early proposal by Pawson and colleagues, i.e., that signalling networks are assembled from conserved interaction modules whose combinatorial deployment confers specificity, robustness, and evolutionary adaptability without reliance on rigid, linear pathways (*39–41*). Our inferred signalling network therefore supports a modular, hierarchical organisation in which control is unevenly distributed across molecular layers and funnelled through preferred pathways under defined conditions.

Notably, many SH2-domain-containing proteins exerted strong functional effects despite limited transcriptional regulation across T-cell activation states. This suggests that signalling control at this level operates largely through constitutively expressed components whose regulatory capacity is governed post-translationally, through phosphorylation, conformational changes, and dynamic recruitment to signalling complexes. As a result, expression-based analyses may underestimate this contribution to signalling control, whereas perturbation-based functional approaches are particularly well suited to reveal their role.

497 Finally, our experimental framework enabled the identification of previously unrecognised
498 negative regulators of T cell effector function, specifically TRRAP and CTDSPL2. TRRAP
499 functions as a core scaffold for multiple histone acetyltransferase complexes, thereby
500 regulating chromatin accessibility and transcriptional output downstream of diverse signalling
501 pathways (*42*). Consistent with this role, TRRAP depletion resulted in coordinated suppression
502 of proliferative and DNA replication–associated transcriptional programs alongside enrichment
503 of inflammatory and immune signalling modules, indicating a redistribution of transcriptional
504 state rather than global activation. In contrast, CTDSPL2 is a poorly characterised
505 serine/threonine phosphatase implicated in transcriptional regulation and cell-state control,
506 and its role in T cell biology has not previously been examined (*43*). Notably, CTDSPL2
507 depletion enhanced cytotoxicity with minimal global transcriptional remodelling, suggesting
508 that its effects are mediated primarily through altered signalling dynamics rather than broad
509 transcriptional reprogramming. These findings provide functional validation of nodes identified
510 in the signalome-wide arrayed perturbation screen and illustrate how this approach can
511 uncover regulatory layers that modulate signalling output and effector potential that may be
512 overlooked by pooled genetic screens.

513 In conclusion, whereas genome-wide perturbation screens and high intensity stimulation-
514 based approaches have been effective for defining essential signalling components, they are
515 less well-suited to dissecting signalling networks dependent on quantitative effects. By
516 emphasising quantitative, time-resolved functional outputs in the setting of physiological
517 stimulation, the framework presented here offers a general strategy for interrogating cell
518 responses as the field moves toward a system-level understanding of signalling.

519 # Materials and Methods

520 ## Cell culture

521 All Jurkat cell lines were cultured in RPMI-1640 medium (Gibco, #21875-034) supplemented
522 with 10% FCS (Gibco, #A5256801, Lot #B3024242RP), 1% Penicillin-Streptomycin-Neomycin
523 (Sigma-Aldrich, #P4083), 1% L-Glutamine (Sigma-Aldrich, #G7513), 1% Sodium Pyruvate
524 (Sigma-Aldrich, #S8636) and 1% HEPES (Gibco, #15630-056). HEK293-T cells for lentivirus
525 production were cultured in DMEM complete medium (Gibco, #41965-039) supplemented as
526 described for the RPMI-1640 Jurkat medium. A375 melanoma cell lines were cultured in
527 DMEM-F12 medium (Gibco, #11320-033) supplemented with 10% FCS, 1% Penicillin-
528 Streptomycin-Neomycin, 1% Sodium Pyruvate and 1% HEPES. Finally, all primary human
529 cells were cultured in RPMI-1640 medium supplemented with 10% human serum, 1%
530 Penicillin-Streptomycin-Neomycin, 1% L-Glutamine, 1% Sodium Pyruvate, 1% non-essential
531 amino acids (NEAA, Gibco, #11140), 1% HEPES and 0.1% B-mercaptoethanol (Gibco,
532 #31350-010).

533 ## Production of 1G4^{+} Jurkat NF-kB GFP reporter cell lines

534 Jurkat T-cells (ATCC) were first transduced with the Cas9 encoding plasmid pKLV2-EF1a-
535 Cas9Bsd-W, as previously described (*26*), to produce Cas9 expressing Jurkat cell lines. Next,
536 Cas9^{+} Jurkat cells were transduced with pSIRV-NF-kB-eGFP construct which was a gift from
537 Peter Steinberger (Addgene plasmid # 118093)(*44*) prior to single cell cloning and selection
538 of NF-kB GFP expressing clones. Endogenous TCR was then deleted from these lines via
539 electroporation with a TRAC/TRBC sgRNA - Cas9 RNP complex. For the generation of RNPs,
540 sgRNAs targeting TRAC and TRBC1/2 (IDT, TRAC sequence:
541 AGAGTCTCTCAGCTGGTACA, TRBC1/2 sequence: GGAGAATGACGAGTGGACCC) (*45*)
542 was pre-incubated with Cas9 (IDT, #10007807) at room temperature for 30 minutes. Here,
543 0.73µL of each sgRNA (400µM) was added to 0.5µL of Cas9 (62µM). Electroporation was

544 then performed using the Lonza P3 Nucleofector kit (Lonza, # V4SP-3096) as per
545 manufacturer's instructions. Briefly, one million Jurkat cells were resuspended in 20µL P3
546 buffer (Lonza, #V4SP-3096), to which the complexed RNP was added. Cells were then moved
547 to one well of a 16-well electroporation strip for electroporation with a Lonza Nucleofector on
548 programme #E0115. Cells were immediately recovered from the electroporation strip by the
549 addition of 80µL of media before returning them to culture. Following deletion of endogenous
550 TCR, Cas9^{+} NF-kB GFP^{+} TCR$^{-/-}$ Jurkats were then transduced with constructs encoding for
551 the 1G4-TCR (*18*) to produce the final 1G4^{+} Cas9^{+} NF-kB GFP^{+} Jurkat cell lines.

552 sgRNA design and cloning

553 To design sgRNA molecules, the top two candidates from CRISPick (Broad Institute) were
554 selected for each gene. sgRNA sequences were purchased as oligos in both forward and
555 reverse orientations (Sigma-Aldrich) prior to annealing, and were then cloned into the BbsI
556 site of the CRISPR sgRNA expression vector pKLV2-U6gRNA5(BbsI)-PGKpuro2ABFPW
557 (Addgene, #67974) as previously described (*46*). All sgRNA sequences produced for the
558 signalome library are displayed in supplementary table 1.

559 Lentivirus production

560 Lentiviruses were prepared by transfecting HEK293T with the sgRNA expression vector.
561 Firstly, 500ng sgRNA expression plasmid was combined with 250ng pMD2.G (Addgene,
562 #12259) and 1.2µg psPAX.2 (Addgene, #12260) in 500µL optiMEM (Gibco, #13985062). To
563 this, 2µL plus reagent (Thermo Fisher, #15338100) was added prior to mixing by inversion
564 and incubation at room temperature for 5 minutes. Next, 6µL lipofectamine-LTX (Thermo
565 Fisher #15338100) was added and the solution was again inverted to mix, prior to incubation
566 at room temperature for 30 minutes. This optiMEM mixture was then added to HEK293T cells
567 in a 6 well plate together with 2mL of DMEM medium supplemented as described above.
568 Lentiviral supernatants were then harvested at 48-72hrs and filtered through a 0.45µm filter.

569 All lentiviruses were either used immediately or stored at -80°C until use, but were never
570 freeze-thawed.

571 Peptide sequences for A375 pulsing

572 Where indicated, A375 melanoma cell lines were pulsed with the following NY-ESO-1
573 altered peptide ligands to induce TCR signalling downstream of the 1G4-TCR. Peptide
574 pulsed A375 cell lines were co-cultured with either Jurkat or primary $CD8^+$ T-cells as
575 indicated, and final peptide concentrations are shown throughout the text. All peptides were
576 ordered from Genscript with a purity >95% and were reconstituted in DMSO upon arrival,
577 stored at -80°C, and never freeze-thawed more than twice. 9V: SLLMWITQV, 3Y:
578 SLYMWITQV, 3I: SLIMWITQV, 6T: SLLMWTTQV. Affinities (K_D) for these NY-ESO-1
579 peptides have been previously described (9V ≅ 7.2μM, 3Y ≅ 30μM, 3I ≅17μM, 6T ≅ 101μM)
580 (*47*). Finally, for experiments utilising bispecific T-cell engagers, A375 cell lines were pulsed
581 with the gp100 peptide (10μg/mL, sequence: YLEPGPVTV) as described, which was also
582 obtained from Genscript at >95% and handled as per the NY-ESO-1 altered peptide ligands.

583 Arrayed screening of the signalome in 1G4-TCR^+ Jurkat reporter cell lines

584 $1x10^5$ 1G4-TCR^+ Jurkat NF-kB GFP reporter cells were transduced with 100μL of the arrayed
585 library lentivirus in a 96-U bottomed plate, in a total of 200μL. Transduction was performed by
586 centrifugation at 800g, 90min, 32°C. After 48hrs, transduced cells were grown in the presence
587 of puromycin (1μg/mL final concentration, Gibco, #A11138-03) to select only transduced cells.
588 At day 7, transduced Jurkat reporter cells were counted via flow cytometry alongside
589 simultaneously ensuring transduction and selection success via expression of the BFP tag in
590 the sgRNA plasmid. All cells were 95-100% BFP^+. Following this counting, all culture volumes
591 across the arrayed library were normalised to allow for consistent cell numbers to be utilised
592 in co-cultures with A375 melanoma cells. Here, A375 melanoma cells were treated with

593 100µg/mL of 6T or 9V NY-ESO-1 peptides (alongside a no peptide control), before plating
594 5,000 cells in 25µL in a 384 well plate (Falcon, #353961), to which 10,000 Jurkat reporter cells
595 were added in 25µL. NF-kB signalling pathway activation downstream of TCR engagement
596 was measured using IncuCyte imaging for 42-48 hours.

597 Arrayed screen analysis in Jurkat cells

598 Raw IncuCyte time-course data from multiple experiments and plates were aggregated and
599 annotated with experimental metadata. Condition labels were harmonized, and control wells
600 were explicitly annotated. For each peptide, signalling output was summarized by calculating
601 the area under the curve (AUC) using trapezoidal integration. Data was collected for a total of
602 699 genes from the 708 targeted with the signalome library, where 9 genes were excluded
603 from AUC analysis due to instrument constraints. AUC values were normalized within each
604 experiment and condition to the median AUC of empty control wells and log2-transformed for
605 downstream analysis.
606
607 Each gene was targeted by two independent gRNAs. Guide-level effects were computed as
608 mean log2-normalized AUC ratios across replicates. Gene-level effects were derived using a
609 rule-based guide collapsing strategy that accounts for guide concordance and effect strength.
610 When guide effects were concordant (AUC within 0.5), their median was used; in cases of
611 strong discordance (particularly when one guide showed a weak effect or when guides had
612 opposite signs) the guide with the larger absolute effect was retained. Guide concordance was
613 assessed using Spearman correlation and same-direction agreement.
614
615 Gene-level effects were computed independently for each stimulation condition (6T and 9V)
616 and compared using Spearman correlation. A composite discordance score integrating effect
617 size differences and sign reversals was used to prioritize condition-specific dependencies.
618 Genes were annotated with functional families and essentiality, and family-level effect
619 distributions were visualized to identify pathway-level trends.

620 ## Primary CD8$^+$ T-cell transduction

621 Primary CD8$^+$ T-cells were isolated from healthy donor leukocyte cones obtained from the
622 NHS blood-transfusion service. CD8$^+$ T-cells were isolated using RosetteSep human CD8$^+$ T-
623 cell enrichment cocktail (StemCell, #15023) as per manufacturer's instructions. Isolated CD8$^+$
624 T-cells were then stimulated for 48 hours prior to transduction with 10µL/mL of CD3/CD28
625 immunocult (StemCell, #10971) and 50U/mL IL-2 (Biolegend, #589104), with cells at 2x10^6/mL
626 and 2mL/well in a 48 well plate. 250µL of Retronectin solution (Takara Bio, #351178) at
627 25µg/mL was added to non-treated 24-well tissue culture plates (Costar, #3738) for 24 hours
628 at 4°C prior to transduction. On the day of transduction, Retronectin solution was removed
629 and plates were blocked by addition of 300µL of 2% BSA in PBS (w/v) for 30 minutes at room
630 temperature. The BSA solution was then removed and wells were washed once in 500µL PBS,
631 before addition of 1.5mL of lentiviral supernatant and centrifugation at 2000g for 90 minutes,
632 32°C, no brake. Following centrifugation, all lentiviral supernatant (except 200-250µL to
633 prevent the well from drying) was removed from the well and 10^6 CD8$^+$ T-cells were seeded
634 into the well in 1mL of complete RPMI with supplementation of IL-2 at 50U/mL. Cells were
635 briefly spun onto the lentiviral coated wells at 2000rpm for 2 minutes, 32°C with the brake
636 applied. Transduction efficiency was assessed 48-72 hours post transduction by measuring
637 BFP expression via flow cytometry. Transduced cells were then selected by the addition of
638 puromycin to 1µg/mL (Gibco, #A11138-03), prior to electroporation with Cas9 protein.

639 ## Electroporation of primary CD8$^+$ T-cells

640 Transduced primary CD8$^+$ T-cells were electroporated with Cas9 protein (IDT, #10007807)
641 once BFP expression had reached >75-80%. Electroporation was performed using the Lonza
642 P3 Primary cell nucleofection kit (Lonza, #V4SP-3096) as per manufacturer's instructions.
643 Here, 10^6 CD8$^+$ T-cells were resuspended in 20µL P3 buffer (Lonza, #V4SP-3096), to which
644 0.5µL Cas9 (62µM stock) was added. CD8$^+$ T-cells were then transferred to 1 well of the 16-
645 well electroporation strip before electroporation on programme #E0115. Immediately after

646 electroporation, cells were recovered by the addition of 80µL of complete RPMI-1640 medium
647 supplemented with 50U/mL IL-2. Cells were then plated across 2 wells in a 96 well-flat
648 bottomed tissue culture plate, each in 200µL with IL-2 at 50U/mL. Cells were maintained at 1-
649 $2x10^6$/mL, in the presence of 50U/mL IL-2 and 1µg/mL puromycin, until day 7 post
650 electroporation at which point functional assays were performed. All sgRNA sequences used
651 in the signalome library are displayed in supplementary table 1. Where indicated, perturbations
652 were also performed with RNPs, using independent and non-overlapping guides (IDT) from
653 the signalome library. Guide sequences used for RNP based perturbations are as follows:
654 TRRAP: AGTGGTCTGGTCAACCACCG, CTDSPL2: TTATTCATCAGCCCACGCGG, LCK:
655 GACCCACTGGTTACCTACGA, LCP2: TGAAGAAGTACCACATCGAT, SLA2:
656 GGGACCGGATCAGACACTAC, scRNA: GTATTACTGATATTGGTGGG.

657 A375 melanoma cytotoxicity and T-cell degranulation assays

658 At day 7 post Cas9 electroporation, $5x10^4$ A375 mOrange$^+$ melanoma cells were plated in
659 100µL in a 96 well-flat bottomed tissue culture plate and pulsed with gp100 peptide at a final
660 concentration of 10µg/mL. Cells were incubated at 37°C for at least 4 hours to allow for cell
661 adherence and antigen presentation. A375 cells were then washed once in PBS before
662 addition of $1x10^5$ CD8$^+$ T-cells in 100µL, and 100µL of the gp100-HLA-A2 - CD3 bispecific
663 engager to final concentrations as indicated. Details of this bispecific T-cell engager have been
664 previously described (*18*). Growth of the A375 melanoma cell line was then tracked for
665 approximately 48 hours via IncuCyte imaging, tracking the A375-expressed mOrange
666 fluorescent protein, allowing for quantification of T-cell mediated cytotoxicity (*26*). CD8$^+$ T-cell
667 degranulation was assessed at 4 hours post co-culture by flow cytometry with staining with
668 the following antibodies: CD8 PeCy7, 1:200, Biolegend #344712, CD107α PE, 1:500,
669 Biolegend #328608 and eBioscience fixable viability dye 780, 1:1000, Thermo Fisher #65-
670 0865-18.

671 ## RNA sequencing in primary CD8$^+$ T-cells

672 To assess transcriptional changes with *TRRAP* perturbation, we first targeted *TRRAP* via
673 lentiviral delivery of sgRNA and electroporation of Cas9 protein as previously described. For
674 these experiments, three primary CD8$^+$ T-cell donors were transduced with lentiviruses
675 encoding the TRRAPg1 sequence, or empty plasmid controls. On day 7 post Cas9
676 electroporation, 5x10^5 CD8$^+$ T-cells were activated on OKT3 coated 48-well tissue culture
677 plates for 3 hours. OKT3-coated tissue culture plates were prepared in advance, where each
678 well was treated with 300µL of Ultra-LEAF OKT3 at 1µg/mL (Biolegend, #317326), or PBS
679 only for unstimulated controls. After 3 hours, cells were recovered, washed in PBS and RNA
680 was extracted using the Qiagen RNA mini kit (#74104) as per manufacturer's instructions.
681 Isolated RNA was then sent to Novogene for NGS. FASTQ files were aligned using STAR
682 version 2.7.3a and quantified using featureCounts version 2.0.6. Ensembl Homo sapiens
683 GRCh38.86 was used as the reference genome. Lowly expressed genes were filtered out,
684 and gene expression distributions of each sample were normalised using edgeR version
685 3.42.2. Differential expression analysis was performed using limma version 3.54.2.
686
687 For experiments investigating transcriptional changes associated with *CTDSPL2*
688 perturbation, primary CD8$^+$ T-cells from two donors were transduced with lentiviruses
689 encoding for the CTDPSL2g1 or CTDSPL2g2 sequences, alongside empty plasmid controls.
690 Again, at day 7 post Cas9 electroporation, T-cells were stimulated as described as per
691 *TRRAP* perturbations. At 3 hours post stimulation on plate-bound OKT3, T-cells were
692 collected and resuspended in 50µL DNA/RNA shield (Zymo Research, #R1100-250) and
693 sent to Plasmidsaurus for NGS. Data handling and analysis was performed by
694 Plasmidsaurus as follows: Quality of the fastq files was assessed using FastQC v0.12.1.
695 Reads were then quality filtered using fastp v0.24.0 with poly-X-tail trimming, 3' quality-
696 based tail trimming, a minimum Phred quality score of 15, and a minimum length
697 requirement of 50bp. Quality-filtered reads were aligned to the reference genome using

698 STAR aligner v2.7.11 with non-canonical splice junction removal and output of unmapped
699 reads, followed by coordinate sorting using samtools v1.22.1. PCR and optical duplicates
700 were removed using UMI-based deduplication with UMIcollapse v1.1.0. Alignment quality
701 metrics, strand specificity, and read distribution across genomic features were assessed
702 using RSeQC v5.0.4 and Qualimap v2.3, with results aggregated into a comprehensive
703 quality control report using MultiQC v1.32. Gene-level expression quantification was
704 performed using featureCounts (subread package v2.1.1) with strand specific-counting,
705 multi-mapping read fractional assignment, exons and three prime UTR as the feature
706 identifiers, and grouped by gene_id. Final gene counts were annotated with gene biotype
707 and other metadata extracted from the reference GTF file.

708 Flow cytometry for assessment of $CD8^+$ T-cell phenotype

709 Genetically perturbed $CD8^+$ T-cells were stimulated on gp100 pulsed A375 melanoma cell
710 lines together with the bispecific T-cell engager as described. At 24 hours post stimulation,
711 T-cells were recovered and transferred to a 96-U bottomed plate before staining with 100µL
712 of antibody mix containing the following antibodies, all used at 1:200 unless otherwise
713 stated: CD8 PE-Cy7, Biolegend, #344750, PD-1 Alexa Fluor 647, Biolegend, #329910,
714 LAG3 FITC, Biolegend, #369308, TIM-3 PE, Biolegend, #345006, 4-1BB BV711, Biolegend,
715 #309832, and eBioscience fixable viability dye 780, 1:1000, Thermo Fisher, #65-0865-18.
716 Surface staining was performed at 4°C for a minimum of 20 minutes, before cells were
717 washed twice and acquired on a BD-LSR Fortessa. Data were then analysed in FlowJo
718 (version 10).

719 CRISPR-Cas9 mediated targeting of the SH2 domain gene family in 720 primary $CD8^+$ T-cells

721 Primary $CD8^+$ T-cells were isolated from healthy donor leukocyte cones and transduced with
722 lentiviruses encoding sgRNA molecules targeting all SH2 domain containing genes as

723 previously described (**Supplementary Table 1**). Due to the size of this family, this analysis
724 was split across 6 independent healthy $CD8^+$ T-cell donors, where each donor was
725 consistently assayed against an internal control sgRNA panel consisting of guides targeting:
726 *LCK*, *LCP2*, *ITK*, *CD8* and *SHC4* together with an empty plasmid control. Following
727 electroporation of Cas9 to induce perturbation of these genes, $CD8^+$ T-cells were co-cultured
728 with gp100 pulsed A375 melanoma cell lines, and the bispecific T-cell engager to a final
729 concentration of 10^{-10}M. Cytotoxic responses of $CD8^+$ T-cells were assessed by measuring
730 A375 melanoma growth, for a period of 48 hours. After 48 hours, $CD8^+$ T-cells were
731 harvested and stained with the following antibody cocktail at 4°C for 20 minutes to assess
732 activation marker expression (CD8 PeCy7, 1:200, Biolegend #344712; CD25 AF647, 1:200,
733 Biolegend #302618; 4-1BB BV711, 1:200, Biolegend #309832; eBioscience fixable viability
734 dye 780, 1:1000, Thermo Fisher #65-0865-18).

735 Donor-donor normalisations in primary $CD8^+$ T-cell killing assays
736 targeting SH2 domain family genes

737 In order to account for differing cytotoxic capacities between all $CD8^+$ T-cell donors used to
738 cover perturbation of the entire SH2 domain gene family, killing curves for each perturbation
739 were first normalised to their corresponding internal negative control for each individual
740 donor. This allows for the effect of targeting any given gene within the family to be compared
741 with other genes in the family that were assayed on separate donors, given the size of the
742 SH2 family. Next, to produce a single quantitative parameter for each gene, the area under
743 the curve (AUC) was calculated for all normalised killing curves using the trapz function from
744 the pracma package in R-studio (version 2024.09.1)(*48*). This analysis produced an
745 individual value for targeting each gene within the family, which was used to determine
746 whether this gene behaved as a negative or positive regulator of $CD8^+$ T-cell responses (**Fig**
747 **3F**).

748 ## Production of primary $CD8^+$ 1G4-TCR^+ T-cells and subsequent
749 cytotoxicity assays

750 $CD8^+$ T-cells isolated from healthy donor leukocyte cones were lentivirally transduced with
751 plasmid encoding for the 1G4-TCR together with a LNGFR tag as previously described (*18*).
752 Next, cells were then stained with TCR Vβ13.1 APC (Biolegend, #362408) and LNGFR FITC
753 (Miltenyi Biotech, #130-113-423) at 1:200 and double positive events were purified by
754 fluorescence-activated cell sorting. At the same time, PBMCs were isolated from three
755 separate healthy donor leukocyte cones, and were subjected to an irradiation dose of 3000rad.
756 Irradiated PBMCs were then centrifuged at 300g for 5 minutes, and resuspended at $2x10^6$/mL
757 in complete RPMI-1640 medium. Equal volumes of PBMCs from each of the three donors was
758 then combined, before supplementation of the mixture with 200U/mL IL-2, 1X PHA (500X
759 stock, Invitrogen, #00-4977-03) and 50ng/mL OKT3 (Biolegend, #), to produce T-cell rapid
760 expansion medium (REM). Approximately $1x10^5$ sorted $LNGFR^+$ TCR $V\beta13.1^+$ $CD8^+$ T-cells
761 was then added to 10mL REM and cultured for 5 days before counting and re-seeding to 10^6
762 cells/mL in complete RPMI-1640 medium with 200U/mL IL-2. Cells were then expanded for a
763 further 10-12 days, maintaining IL-2 concentrations at 200U/mL and cell densities at 1-
764 $2x10^6$/mL throughout. Resultant $CD8^+$ T-cell cultures were checked for purity via flow
765 cytometry and staining with CD8 PeCy7, TCR Vβ13.1 APC and LNGFR FITC. Functional
766 reactivity was then assessed by co-culture with NY-ESO-1 expressing A375 cell lines prior to
767 cryopreservation.

768 ## IFN_γ ELISAs

769 Supernatants were collected at 24 hours post $CD8^+$ T-cell and A375 co-culture, and IFN_γ
770 secretion from $CD8^+$ T-cells into the culture supernatant was assessed by ELISA as per
771 manufacturer's instructions (Biolegend, #430101). Supernatants were either used fresh in
772 ELISAs, or were stored at -20°C prior to analysis but were never freeze-thawed.

773 ## CyTOF sample preparation and data analysis

774 A375 cells were plated in 96-well flat-bottom plates at 5 × 10^4 cells per well and pulsed with
775 gp100 peptide (10µg/mL) for a minimum of 4 hours. After peptide loading, cells were washed
776 once with PBS and either incubated with the bispecific T-cell engager at a final concentration
777 of 10^{-10}M or left untreated. Where applicable, bispecific binding was allowed to proceed for at
778 least 30 minutes at 37 °C prior to initiation of the experiment.

779 Isolated $CD8^+$ T cells were subsequently added to either gp100-pulsed bispecific-coated
780 (stimulated) or uncoated (unstimulated) A375 cells and centrifuged (500 g, 1 min) to promote
781 cell contact and initiate activation. At the end of the time course, cells were transferred to 96-
782 well U-bottom plates, pelleted in ice-cold PBS (1800 rpm, 3 min), and fixed in 100 µl of 1.6%
783 PFA. Fixation was carried out at 4 °C for a minimum of 20 minutes, followed by three washes
784 with 200 µl PBS.

785 Mass cytometric analysis was performed as previously described. Briefly, dead cells were
786 labelled with 0.25 mM ^{194}Cisplatin (Standard BioTools, Cat# 201194), after which cells were
787 incubated overnight at 4 °C with thiol-reactive barcodes. Excess barcodes were quenched
788 using 2 mM GSH and samples were pooled. Cells were then washed in cell staining buffer
789 (CSB; Standard BioTools, Cat# 201068) and stained with extracellular rare-earth metal-
790 conjugated antibodies for 30 minutes at room temperature. Cells were then permeabilised with
791 0.1% (v/v) Triton X-100/PBS and 50% methanol/PBS prior to staining with intracellular rare-
792 earth metal-conjugated antibodies for 30 minutes at room temperature. Antibodies were cross-
793 linked using 1.6% (v/v) FA/PBS for 10 minutes. Cells were subsequently incubated overnight
794 at 4 °C with 125 nM ^{191}Ir/^{193}Ir DNA intercalator, washed, resuspended in CAS+ supplemented
795 with 2 mM EDTA, and analysed on a CyTOF XT at 200–400 events per second.

796 Signal intensities were measured by CyTOF at 1, 5, 10, 15, 30, 45, 60, and 120 minutes post-
797 stimulation using a panel of 42 markers. Raw data were preprocessed in FlowJo and

798 subsequently analysed using the CyGNAL python package (github.com/TAPE-
799 Lab/CyGNAL(*14*)) with default settings.

800 Analysis of published RNA expression and CRISPR dataset

801 To obtain the lists of signalome genes that were regulated during T cell activation, raw counts
802 of bulk RNA sequencing dataset were downloaded from Gene Expression Omnibus (GEO).
803 We filtered the data for CD8+ T cells except for GSE197067, where only pan-T cells were
804 analyzed. Gene IDs were mapped to gene names by mygene package (Python). Data was
805 prefiltered by subsetting for genes that have at least 10 counts in more than 20% of samples.
806 Differential expression analysis was performed using DESeq2 (R)(*49*) using appropriate
807 model design for study and p values were obtained with the wald test. Log fold change (LFC)
808 was shrunk with the apeglm method to reduce inflation of lowly expressed genes. Differentially
809 expressed genes (DEGs) were obtained by thresholding for adjusted p-value < 0.001, and
810 LFC < 1.5. DEGs of different conditions (e.g. timepoints) of the same dataset were merged by
811 their union and intersected with our signalome gene list. To obtain the lists of signalome genes
812 that were identified as hits in pooled CRISPR screening, we downloaded the processed result
813 files from each study, thresholded the hits following the description of each study and
814 intersected with our signalome gene list.
815
816

References

1. B. M. Invergo, P. Beltrao, Reconstructing phosphorylation signalling networks from quantitative phosphoproteomic data. *Essays Biochem.* **62**, 525–534 (2018).

2. E. J. Needham, B. L. Parker, T. Burykin, D. E. James, S. J. Humphrey, Illuminating the dark phosphoproteome. *Sci. Signal.* **12**, eaau8645 (2019).

3. M. Locard-Paulet, G. Voisinne, C. Froment, M. Goncalves Menoita, Y. Ounoughene, L. Girard, C. Gregoire, D. Mori, M. Martinez, H. Luche, J. Garin, M. Malissen, O. Burlet-Schiltz, B. Malissen, A. Gonzalez de Peredo, R. Roncagalli, LymphoAtlas: a dynamic and integrated phosphoproteomic resource of TCR signaling in primary T cells reveals ITSN2 as a regulator of effector functions. *Mol. Syst. Biol.* **16**, e9524 (2020).

4. R. N. Joshi, N. A. Binai, F. Marabita, Z. Sui, A. Altman, A. J. R. Heck, J. Tegnér, A. Schmidt, Phosphoproteomics reveals regulatory T cell-mediated DEF6 dephosphorylation that affects cytokine expression in human conventional T cells. *Front. Immunol.* **8**, 1163 (2017).

5. P. Ruperez, A. Gago-Martinez, A. L. Burlingame, J. A. Oses-Prieto, Quantitative phosphoproteomic analysis reveals a role for serine and threonine kinases in the cytoskeletal reorganization in early T cell receptor activation in human primary T cells. *Mol. Cell. Proteomics* **11**, 171–186 (2012).

6. R. B. Kitata, W.-K. Choong, C.-F. Tsai, P.-Y. Lin, B.-S. Chen, Y.-C. Chang, A. I. Nesvizhskii, T.-Y. Sung, Y.-J. Chen, A data-independent acquisition-based global phosphoproteomics system enables deep profiling. *Nat. Commun.* **12**, 2539 (2021).

7. P. Mertins, NCI CPTAC, D. R. Mani, K. V. Ruggles, M. A. Gillette, K. R. Clauser, P. Wang, X. Wang, J. W. Qiao, S. Cao, F. Petralia, E. Kawaler, F. Mundt, K. Krug, Z. Tu, J. T. Lei, M. L. Gatza, M. Wilkerson, C. M. Perou, V. Yellapantula, K.-L. Huang, C. Lin, M. D. McLellan, P. Yan, S. R. Davies, R. R. Townsend, S. J. Skates, J. Wang, B. Zhang, C. R. Kinsinger, M. Mesri, H. Rodriguez, L. Ding, A. G. Paulovich, D. Fenyö, M. J. Ellis, S. A. Carr, Proteogenomics connects somatic mutations to signalling in breast cancer. *Nature* **534**, 55–62 (2016).

8. V. Cordo', M. T. Meijer, R. Hagelaar, R. R. de Goeij-de Haas, V. M. Poort, A. A. Henneman, S. R. Piersma, T. V. Pham, K. Oshima, A. A. Ferrando, G. J. R. Zaman, C. R. Jimenez, J. P. P. Meijerink, Phosphoproteomic profiling of T cell acute lymphoblastic leukemia reveals targetable kinases and combination treatment strategies. *Nat. Commun.* **13**, 1048 (2022).

9. A. Subramanian, R. Narayan, S. M. Corsello, D. D. Peck, T. E. Natoli, X. Lu, J. Gould, J. F. Davis, A. A. Tubelli, J. K. Asiedu, D. L. Lahr, J. E. Hirschman, Z. Liu, M. Donahue, B. Julian, M. Khan, D. Wadden, I. C. Smith, D. Lam, A. Liberzon, C. Toder, M. Bagul, M. Orzechowski, O. M. Enache, F. Piccioni, S. A. Johnson, N. J. Lyons, A. H. Berger, A. F. Shamji, A. N. Brooks, A. Vrcic, C. Flynn, J. Rosains, D. Y. Takeda, R. Hu, D. Davison, J. Lamb, K. Ardlie, L. Hogstrom, P. Greenside, N. S. Gray, P. A. Clemons, S. Silver, X. Wu, W.-N. Zhao, W. Read-Button, X. Wu, S. J. Haggarty, L. V. Ronco, J. S. Boehm, S. L. Schreiber, J. G. Doench, J. A. Bittker, D. E. Root, B. Wong, T. R. Golub, A next generation Connectivity Map: L1000 platform and the first 1,000,000 profiles. *Cell* **171**, 1437–1452.e17 (2017).

10. S. Ibáñez-Molero, J. T. M. Pruijs, A. Atmopawiro, F. Wang, A. M. Terry, M.

861 Altelaar, D. S. Peeper, K. E. Stecker, Phosphoprotein dynamics of interacting T cells
862 and tumor cells by HySic. *Cell Rep.* **43**, 113598 (2024).

863 11. M. N. Navarro, J. Goebel, C. Feijoo-Carnero, N. Morrice, D. A. Cantrell,
864 Phosphoproteomic analysis reveals an intrinsic pathway for the regulation of histone
865 deacetylase 7 that controls the function of cytotoxic T lymphocytes. *Nat. Immunol.* **12**,
866 352–361 (2011).

867 12. G. Franciosa, A. W. P. Jensen, A. Martinez-Val, I. Piga, M. Donia, J. V.
868 Olsen, The proteomics and phosphoproteomics landscape of melanoma under T cell
869 attack, *bioRxiv* (2025). https://doi.org/10.1101/2025.09.12.675787.

870 13. A. S. Tocheva, M. Peled, M. Strazza, K. R. Adam, S. Lerrer, S. Nayak, I.
871 Azoulay-Alfaguter, C. J. R. Foster, E. A. Philips, B. G. Neel, B. Ueberheide, A. Mor,
872 Quantitative phosphoproteomic analysis reveals involvement of PD-1 in multiple T cell
873 functions. *J. Biol. Chem.* **295**, 18036–18050 (2020).

874 14. J. Sufi, X. Qin, F. C. Rodriguez, Y. J. Bu, P. Vlckova, M. R. Zapatero, M. Nitz,
875 C. J. Tape, Multiplexed single-cell analysis of organoid signaling networks. *Nat. Protoc.*
876 **16**, 4897–4918 (2021).

877 15. C. B. Nattress, R. O'Sullivan, D. Fowler, C. Hutton, P. Vlckova, J. Sufi, M.
878 Buschhaus, E. Basiarz, M. Ramos Zapatero, F. Cardoso Rodriguez, X. Qin, A.
879 Campbell, A. Kanouta, V. S. W. Li, K. Chester, J. Anderson, M. Barisa, J. P. H. Fisher,
880 C. J. Tape, Phenoscaping reveals multimodal γδ T-cell cytotoxicity as a strategy to
881 overcome cancer cell-mediated immunomodulation. *Cancer Res.* **85**, 4415–4432
882 (2025).

883 16. X. Qin, F. Cardoso Rodriguez, J. Sufi, P. Vlckova, J. Claus, C. J. Tape, An
884 oncogenic phenoscape of colonic stem cell polarization. *Cell* **186**, 5554–5568.e18
885 (2023).

886 17. S. Krishnaswamy, M. H. Spitzer, M. Mingueneau, S. C. Bendall, O. Litvin, E.
887 Stone, D. Pe'er, G. P. Nolan, Systems biology. Conditional density-based analysis of T
888 cell signaling in single-cell data. *Science* **346**, 1250689 (2014).

889 18. M. Kotowski, D. F. Heraghty, M. Körbel, D. Banik, Z. Zhang, S. Kedia, B. Fu,
890 J. McColl, B. Li, J. Clarke, M. Fellermeyer, Y. Lui, G. Bossi, D. K. Cole, H. Chen, E.
891 Basiarz, S. Sharma, E. Petsalaki, C. J. Tape, B. de Wet, S. F. Lee, A. M. Santos, D.
892 Klenerman, S. J. Davis, T-cell signaling relies on partial CD45-exclusion at sub-micron
893 sized cellular contacts, bioRxiv (2025).
894 https://www.biorxiv.org/content/10.1101/2025.08.29.673015v1.

895 19. N. Moret, C. Liu, B. M. Gyori, J. A. Bachman, A. Steppi, C. Hug, R. Taujale,
896 L.-C. Huang, M. E. Berginski, S. M. Gomez, N. Kannan, P. K. Sorger, Exploring the
897 understudied human kinome for research and therapeutic opportunities, bioRxiv (2020);
898 https://doi.org/10.37473/fic/10.1101/2020.04.02.022277

899 20. D. van der Meer, S. Barthorpe, W. Yang, H. Lightfoot, C. Hall, J. Gilbert, H. E.
900 Francies, M. J. Garnett, Cell Model Passports-a hub for clinical, genetic and functional
901 datasets of preclinical cancer models. *Nucleic Acids Res.* **47**, D923–D929 (2019).

902 21. M. Kanehisa, M. Furumichi, Y. Sato, Y. Matsuura, M. Ishiguro-Watanabe,
903 KEGG: biological systems database as a model of the real world. *Nucleic Acids Res.*
904 **53**, D672–D677 (2025).

22. N. G. Bediaga, H. D. Coughlan, T. M. Johanson, A. L. Garnham, G. Naselli, J. Schröder, L. G. Fearnley, E. Bandala-Sanchez, R. S. Allan, G. K. Smyth, L. C. Harrison, Multi-level remodelling of chromatin underlying activation of human T cells. *Sci. Rep.* **11**, 528 (2021).

23. J. Ogando, M. E. Sáez, J. Santos, C. Nuevo-Tapioles, M. Gut, A. Esteve-Codina, S. Heath, A. González-Pérez, J. M. Cuezva, R. A. Lacalle, S. Mañes, PD-1 signaling affects cristae morphology and leads to mitochondrial dysfunction in human CD8+ T lymphocytes. *J. Immunother. Cancer* **7**, 151 (2019).

24. M. Rade, S. Böhlen, V. Neuhaus, D. Löffler, C. Blumert, M. Merz, U. Köhl, S. Dehmel, K. Sewald, K. Reiche, A time-resolved meta-analysis of consensus gene expression profiles during human T-cell activation. *Genome Biol.* **24**, 287 (2023).

25. Y. Lui, E. Jenkins, E. Z. Q. Ng, M. Kotowski, S. J. Mullin, J. Clarke, S. J. Davis, A. M. Santos, S. Sharma, Cell state and transcription factor modulation during extended ex vivo CD8 + T-cell expansion, bioRxiv. (2024). https://www.biorxiv.org/content/10.1101/2024.07.17.603780v1.full.

26. S. Sharma, T. Whitehead, M. Kotowski, E. Z. Q. Ng, J. Clarke, J. Leitner, Y.-L. Chen, A. M. Santos, P. Steinberger, S. J. Davis, A high-throughput two-cell assay for interrogating inhibitory signaling pathways in T cells. *Life Sci Alliance* **7** (2024).

27. E. Shifrut, J. Carnevale, V. Tobin, T. L. Roth, J. M. Woo, C. T. Bui, P. J. Li, M. E. Diolaiti, A. Ashworth, A. Marson, Genome-wide CRISPR Screens in Primary Human T Cells Reveal Key Regulators of Immune Function. *Cell* **175**, 1958–1971.e15 (2018).

28. J. Carnevale, E. Shifrut, N. Kale, W. A. Nyberg, F. Blaeschke, Y. Y. Chen, Z. Li, S. P. Bapat, M. E. Diolaiti, P. O'Leary, S. Vedova, J. Belk, B. Daniel, T. L. Roth, S. Bachl, A. A. Anido, B. Prinzing, J. Ibañez-Vega, S. Lange, D. Haydar, M. Luetke-Eversloh, M. Born-Bony, B. Hegde, S. Kogan, T. Feuchtinger, H. Okada, A. T. Satpathy, K. Shannon, S. Gottschalk, J. Eyquem, G. Krenciute, A. Ashworth, A. Marson, RASA2 ablation in T cells boosts antigen sensitivity and long-term function. *Nature* **609**, 174–182 (2022).

29. R. Schmidt, Z. Steinhart, M. Layeghi, J. W. Freimer, R. Bueno, V. Q. Nguyen, F. Blaeschke, C. J. Ye, A. Marson, CRISPR activation and interference screens decode stimulation responses in primary human T cells. *Science* **375**, eabj4008 (2022).

30. J. Cabezas-Caballero, A. Huhn, M. A. Kutuzov, V. Andre, A. Shomuradova, B. W. A. Peeters, G. M. Gillespie, P. A. van der Merwe, O. Dushek, Generation of T cells with reduced off-target cross-reactivities by engineering co-signalling receptors. *Nat. Biomed. Eng.*, doi: 10.1038/s41551-025-01563-w (2026).

31. J. O. Valenzuela, C. Iclozan, M. S. Hossain, M. Prlic, E. Hopewell, C. C. Bronk, J. Wang, E. Celis, R. W. Engelman, B. R. Blazar, M. J. Bevan, E. K. Waller, X.-Z. Yu, A. A. Beg, PKCtheta is required for alloreactivity and GVHD but not for immune responses toward leukemia and infection in mice. *J. Clin. Invest.* **119**, 3774–3786 (2009).

32. E. Güç, A. Treveil, E. Leach, A. Broomfield, A. Camera, J. Clubley, P. Nieto Garcia, A. Kazachenka, R. Khanolkar, L. Del Carpio, H. Heyn, J. C. Hassel, J. J. Sacco, S. Stanhope, L. Collins, J. M. Piulats, K. Ranade, A. Benlahrech, Tebentafusp, a T cell engager, promotes macrophage reprogramming and in combination with IL-2 overcomes macrophage immunosuppression in cancer. *Nat. Commun.* **16**, 2374 (2025).

950 33. J. Harper, K. J. Adams, G. Bossi, D. E. Wright, A. R. Stacey, N. Bedke, R.
951 Martinez-Hague, D. Blat, L. Humbert, H. Buchanan, G. S. Le Provost, Z. Donnellan, R.
952 J. Carreira, S. J. Paston, L. U. Weigand, M. Canestraro, J. P. Sanderson, S. Botta
953 Gordon-Smith, K. L. Lowe, K. A. Rygiel, A. S. Powlesland, A. Vuidepot, N. J. Hassan, B.
954 J. Cameron, B. K. Jakobsen, J. Dukes, An approved in vitro approach to preclinical
955 safety and efficacy evaluation of engineered T cell receptor anti-CD3 bispecific
956 (ImmTAC) molecules. *PLoS One* **13**, e0205491–e0205491 (2018).

957 34. J. E. Purvis, G. Lahav, Encoding and decoding cellular information through
958 signaling dynamics. *Cell* **152**, 945–956 (2013).

959 35. M. J. Harris, M. Fuyal, J. R. James, Quantifying persistence in the T-cell
960 signaling network using an optically controllable antigen receptor. *Mol. Syst. Biol.* **17**,
961 e10091 (2021).

962 36. S. C. Bendall, E. F. Simonds, P. Qiu, E.-A. D. Amir, P. O. Krutzik, R. Finck, R.
963 V. Bruggner, R. Melamed, A. Trejo, O. I. Ornatsky, R. S. Balderas, S. K. Plevritis, K.
964 Sachs, D. Pe'er, S. D. Tanner, G. P. Nolan, Single-cell mass cytometry of differential
965 immune and drug responses across a human hematopoietic continuum. *Science* **332**,
966 687–696 (2011).

967 37. H. Dada, M. L. Dustin, Goldilocks and the three TILs. *J. Exp. Med.* **219**
968 (2022).

969 38. V. Horkova, A. Drobek, D. Paprckova, V. Niederlova, A. Prasai, V. Uleri, D.
970 Glatzova, M. Kraller, M. Cesnekova, S. Janusova, E. Salyova, O. Tsyklauri, T. A.
971 Kadlecek, K. Krizova, R. Platzer, K. Schober, D. H. Busch, A. Weiss, J. B. Huppa, O.
972 Stepanek, Unique roles of co-receptor-bound LCK in helper and cytotoxic T cells. *Nat.*
973 *Immunol.* **24**, 174–185 (2023).

974 39. T. Pawson, J. D. Scott, Signaling through scaffold, anchoring, and adaptor
975 proteins. *Science* **278**, 2075–2080 (1997).

976 40. T. Pawson, P. Nash, Assembly of cell regulatory systems through protein
977 interaction domains. *Science* **300**, 445–452 (2003).

978 41. W. A. Lim, T. Pawson, Phosphotyrosine signaling: evolving a new cellular
979 communication system. *Cell* **142**, 661–667 (2010).

980 42. D. Detilleux, P. Raynaud, B. Pradet-Balade, D. Helmlinger, The TRRAP
981 transcription cofactor represses interferon-stimulated genes in colorectal cancer cells.
982 *Elife* **11**, e69705 (2022).

983 43. M. Li, L. Chen, F. Yu, H. Mei, X. Ma, K. Ding, Y. Yang, Z. Rong, CTDSPL2
984 promotes the progression of non-small lung cancer through PI3K/AKT signaling via
985 JAK1. *Cell Death Discov.* **10**, 389 (2024).

986 44. S. Jutz, A. Hennig, W. Paster, Ö. Asrak, D. Dijanovic, F. Kellner, W. F. Pickl,
987 J. B. Huppa, J. Leitner, P. Steinberger, A cellular platform for the evaluation of immune
988 checkpoint molecules. *Oncotarget* **8**, 64892–64906 (2017).

989 45. Y.-L. Chen, J. S. W. Ng, R. Ottakandathil Babu, J. Woo, J. Nahler, C. S.
990 Hardman, P. Kurupati, L. Nussbaum, F. Gao, T. Dong, K. Ladell, D. A. Price, D. A.
991 Duncan, D. Johnson, U. Gileadi, H. Koohy, G. S. Ogg, Group A Streptococcus induces
992 CD1a-autoreactive T cells and promotes psoriatic inflammation. *Sci. Immunol.* **8**,
993 eadd9232 (2023).

46. S. Sharma, G. J. Wright, *Cell Surface Receptor Identification Using Genome-Scale CRISPR/Cas9 Genetic Screens* (2020; https://www.jove.com/t/60803/cell-surface-receptor-identification-using-genome-scale-crisprcas9).

47. M. Aleksic, O. Dushek, H. Zhang, E. Shenderov, J.-L. Chen, V. Cerundolo, D. Coombs, P. A. van der Merwe, Dependence of T cell antigen recognition on T cell receptor-peptide MHC confinement time. *Immunity* **32**, 163–174 (2010).

48. H. W. Borchers, *Pracma: Practical Numerical Math Functions* (https://cran.r-project.org/web/packages/pracma/index.html).

49. M. I. Love, W. Huber, S. Anders, Moderated estimation of fold change and dispersion for RNA-seq data with DESeq2, *bioRxiv* (2014). https://doi.org/10.1101/002832.

Author contribution:

The experiments were conceived by S.S, E.P, S.J.D, and C.J.T, and the methodology developed by J.C and S.S. The experimental work was undertaken by J.C, S.S, C.T.G, E.B, M.K, A.M.S, M.T. V, P.S, J.X.L. Data analysis was performed by J.C, H.C, and S.S. The work was supervised by S.S, E.P, S.J.D, C.J.T, and funding was acquired by J.C, S.S, E.P, S.J.D, C.J.T. The original manuscript was written by J.C, S.S, and E.P and revised by H.C, M.K, A.M.S, C.J.T and S.J.D.

Acknowledgements

This work was funded by MRC (grant MR/W025507/1 to E.P., S.S., C.T., and S.J.D.) and Wellcome grant to S.S (317519/Z/24/Z), and MSIF pump priming grant to J.C (BRDNB420).